

Influence of climate change on precipitation extremes in Ecuador

Katy Valdivieso-García 1,2 · Angel Vázquez-Patiño 3,4,5 · Hugo Saritama · Luan Contreras · Alex Avilés 1,2 · Fernando García 1,2 ·

Received: 8 May 2023 / Accepted: 21 October 2024

© The Author(s), under exclusive licence to Springer Nature B.V. 2024

Abstract

Understanding the spatiotemporal variability of extreme precipitation is crucial for risk management. The effects of climate change can increase the frequency and severity of these extremes, generating more environmental hazards. Although there is research about climate extremes in specific areas of Ecuador, knowledge of extreme precipitation on an entire national scale still needs to be available. This study contributes to this gap by comprehensively evaluating continental Ecuador's precipitation extremes. Climate precipitation indices of the Group of Experts on Detection and Climate Change Indices (ETCCDI) are assessed with observed data and future data derived from projections of regional climate models of Ecuador in two Representative Concentration Pathways (RCP), 4.5 and 8.5. Ground meteorological data and the MSWEP satellite product are merged by applying a Random Forest-based methodology (RF-MEP) to generate an observations data grid (1981-2015) containing the spatiotemporal distribution of precipitation throughout Ecuador. On the other hand, the future projections (2016-2070) are bias-corrected through statistical downscaling using Quantile Delta Mapping (QMD). Consequently, eleven extreme precipitation indices are evaluated, and trends with the Mann-Kendall test are analyzed. The results show an increase in total rainfall and intensities, especially in the north and center of the Coast and the Amazon, with a maximum of approximately 32 mm/year in the RCP 8.5 scenario. This scenario presents significantly increasing precipitation trends in all regions on highly wet days. Some notable indices are the days of heavy rain greater than 10 and 20 mm, which would increase in the future scenarios to 148 and 76 days/ year, respectively, especially in some areas of the center and north of the Amazon and the north of the Coast. The present research fills knowledge gaps of extreme precipitation trends in Ecuador that could assist decision-makers in applying measures for climatic threat reduction.

Keywords Extreme precipitation future projections · ETCCDI indices · Regional climate models · Ecuador

Extended author information available on the last page of the article

Published online: 07 November 2024



165 Page 2 of 22 Climatic Change (2024) 177:165

1 Introduction

Climate change is considered a global phenomenon; however, its effects and impacts occur on a local or regional scale. One of the most relevant effects expected is the modification of weather patterns and the increased frequency of extreme events related to the spatiotemporal distribution of precipitation (Palmer and Räisänen 2002), producing floods and droughts (Leng et al. 2015). These threats cause social, economic, and environmental impacts that would intensify regarding climate change (Useros 2013; Uribe 2017). In recent decades, extreme weather events have been recognized worldwide as imperative triggers of hydroclimatic threats, becoming an increasingly important study area (Sisco et al. 2017; Gentilucci et al. 2020).

Most research has focused on analyzing and monitoring climate trends and extreme events employing precipitation-based climate indices (Alexander and Tebaldi 2012; Milanovic et al. 2015; Touré Halimatou et al. 2017). The Expert Team on Climate Change Detection and Indices (ETCCDI) determined a set of eleven standardized indices derived from daily precipitation data for the assessment of the variability of extreme climate events around the planet (Karl et al. 1999; Peterson et al. 2001; Zhang and Yang 2004). A more detailed description of the indices can be found at etccdi.pacificclimate.org/list_27_indices. shtml. Applying and analyzing these indices in a given area can be a tool to assess the variability of precipitation extremes, providing information to identify climate threats and anticipate mitigation actions (Cuartas et al. 2017; Torres Pineda and Pabón Caicedo 2017; Esquivel et al. 2018).

In recent years, Ecuador has experienced weather patterns that affected significant economic activities such as agriculture, fishing, and using natural resources, as they depend directly on the climate (Yánez et al. 2011). This issue has encouraged research on climate variability and climate extremes in specific areas of Ecuador. For instance, Serrano Vincenti et al. (2016) showed that the city of Machala, located in the coastal region, has a high risk of flooding due to extreme precipitation, which could increase in intensity and frequency due to the influence of the El Niño Southern Oscillation (ENSO) phenomenon and climate change. The Andean region's hydrological balance is currently being threatened by climate variability, which leads to severe consequences for living beings (Kinouchi et al. 2019). Serrano Vincenti et al. (2012) analyzed the impact of climate change and climate variability on the Metropolitan District of Quito by applying ETCCDI indices. The study showed an increase in anomalous trends and behaviors in precipitation that can be considered a consequence of climate change. Similarly, Montenegro et al. (2022), in their study of the Paute river basin in the Ecuadorian Andes, determined an increment of maximum precipitation for RCP 4.5 and 8.5 projections of CMIP5 models. In contrast, the Amazon Cooperation Treaty Organization presented the results of high-resolution regional and global climate models suggesting a decrease in precipitation in the Central and Eastern Amazon by the end of the 21st century (Scholze 2014).

Despite studies on climatic extremes in specific Ecuadorian regions, comprehensive data generation for the entire country still needs to be improved. Ballari et al. (2018) analyzed the spatiotemporal dependencies of precipitation to regionalize the seasonality and intensity of precipitation in Ecuador. However, this analysis was performed only with historical information. On the other hand, Campozano et al. (2020) used precipitation projections from regional climate models derived from CMIP5 models and determined a decrease in droughts



Climatic Change (2024) 177:165 Page 3 of 22 165

in mainland Ecuador. They found that these models show high bias between simulated and observed data. Such issues show that data correction is essential, which was performed in this study.

The objective of the study was to analyze the spatiotemporal variations in precipitation extremes in Ecuador through the evaluation of eleven ETCCDI precipitation indices with observed information and projections of the regional climate model of the Third Communication on Climate Change of Ecuador (MAE-PNUD 2017) in two scenarios based on representative concentration pathways (RCP) 4.5 and 8.5.

2 Study area

The study area is continental Ecuador, with an area of 248,513 km². Ecuador is located northwest of South America (Fig. 1a) and comprises three regions: Coast, Andes, and Amazon (Fig. 1b). Due to its geographical location, Ecuador has a great variety of climatic conditions throughout its territory, precipitation being the climatic variable with the most significant variability. In the Coast region, precipitation tends to increase due to events associated with the El Niño 1 + 2 phenomenon and the intertropical convergence zone (ITCZ) (Tobar and Wyseure 2018; Ballari et al. 2018; Thielen et al. 2023), resulting in rainy seasonality from December to April (Campozano et al. 2016). In the Andean region, due to the oro-

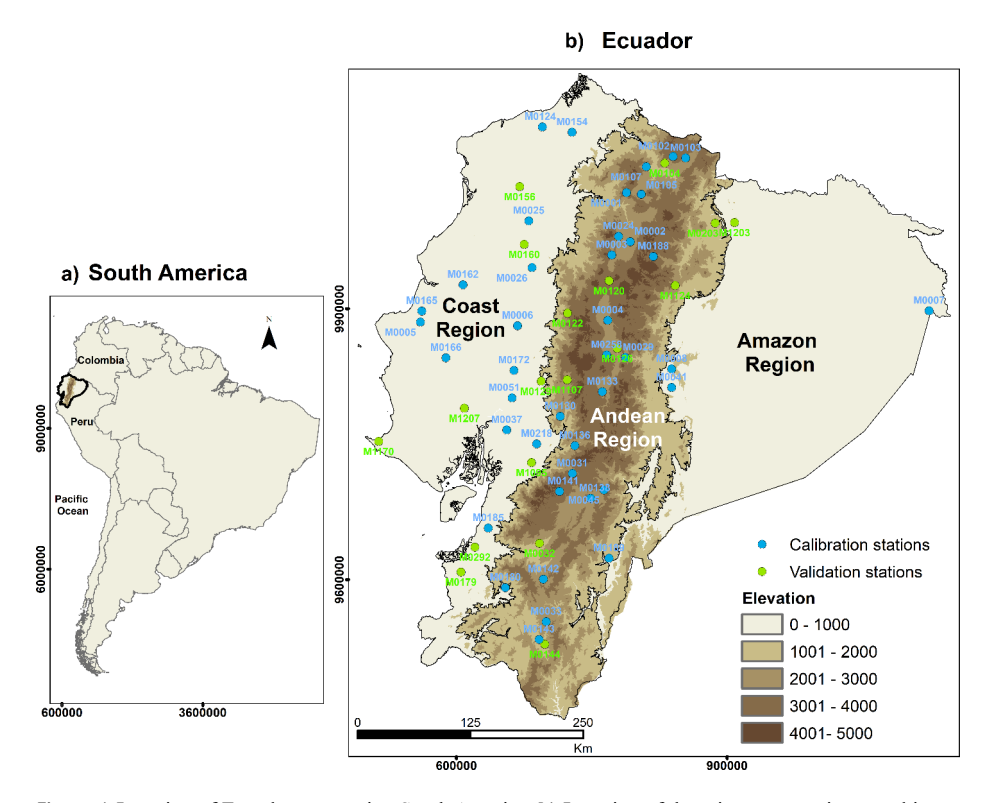


Fig. 1 a) Location of Ecuador concerning South America, b) Location of the rain gauge stations used in the study



165 Page 4 of 22 Climatic Change (2024) 177:165

graphic effects of the Andes mountain range, a bimodal rain regime is induced, with a dry period from June to September (Ulloa et al. 2017). Finally, in the Amazon, a rainy pattern is generated throughout the year, with two well-defined periods in March-April and October-November, regulated by the humid air of the Amazon basin and the ITCZ (Campozano et al. 2016; Ulloa et al. 2017).

3 Data

3.1 In-situ data for gridded precipitation products calibration and validation

Daily precipitation data from 73 rain gauges distributed throughout continental Ecuador between 1981 and 2015 were obtained from the National Institute of Meteorology and Hydrology of Ecuador (INAMHI). Data were subjected to a rigorous quality control procedure performed in two groups. First, rain gauges were divided into two datasets, one for calibrating gridded precipitation products and another for validating the calibration procedure. Rain gauges with at least 80% of existing data during the study period were considered candidate stations for calibration following the recommendations of the World Meteorological Organization (2018) for climate studies. Other criteria, such as excluding stations with more than three consecutive missing years, were not considered in our study. We omitted this criterion due to the limited number of stations with complete datasets in our study area, significantly reducing the number of rain gauges for properly calibrating gridded products. On the other hand, the remaining rain gauges (with less than 80% of data) were considered potential validation stations. It is important to note that this selection leads to an inhomogeneous spatial distribution of rain gauges for the validation procedure, especially in the north-central part of the Coast region. However, we think that this spatial distribution does not significantly affect the performance of the validation results due to precipitation in this region being quite homogeneous (Ballari et al. 2018; Ilbay-Yupa et al. 2021).

The quality control applied to the group of calibration stations was based on checking the homogeneity of the time series using double-mass curves according to proximity criteria among rain gauges in this group. In contrast, the nearest calibration station was considered the reference for the validation stations. This procedure removed stations that had strange and suspicious behaviors and resulted in 41 calibration and 18 validation stations (Fig. 1b). Finally, to use the same number of calibration stations at each time step, missing data for the calibration stations were filled using the orthogonal regression model considering the proximity and high correlation between stations. The quality check of data and the estimation of missing values were performed using the 'climatol' R package (Guijarro 2018).

3.2 Gridded precipitation products

Two widely used precipitation products were considered to analyze the spatio-temporal variability of precipitation extremes throughout Ecuador: the Climate Hazards Group Infrared Precipitation with Stations version 2 (CHIRPS V2.0) and the Multi-Source Weighted-Ensemble Precipitation version 2.2 (MSWEP V2.2). These datasets were selected over other products due to their long-term data and relatively high spatial resolution (ranging from 0.05° to 0.1°, respectively), making them suitable for better characterization of precipitation patterns



Climatic Change (2024) 177:165 Page 5 of 22 165

at regional and local scales. Both products combine multiple satellites, reanalysis, and available in-situ observations, which have shown an overall high performance in the region in comparison to other precipitation products (Baez-Villanueva et al. 2018; Fernandez-Palomino et al. 2022; Valencia et al. 2023). Both datasets were freely downloaded at a daily time scale for the period 1981-2015 from the CHIRPS V2.0 (https://www.chc.ucsb.edu/data/chirps) and the MSWEP V2.2 (https://www.gloh2o.org/mswep/) websites. Detailed information about CHIRPS V2.0 and MSWEP V2.2 precipitation products can be found in Funk et al. (2015) and Beck et al. (2019), respectively.

3.3 Precipitation projections

Precipitation simulations (in the historical and future periods) were obtained from the Third National Communication on Climate Change performed by the Ministry of Environment, Water and Ecological Transition (MAATE) (Armenta et al. 2016). Four modeled precipitation datasets were created by Armenta et al. (2016), dynamically downscaling from Global Circulation Models (GCMs) CSIRO-Mk3-6.0, GISS-E2-R, IPSL-CM5A-MR, and MIROC-ESM (the best ones for Ecuador from the CMIP5 project), through of Weather Research and Forecasting model (WRF). In addition, Armenta et al. (2016) developed an ensemble Regional Climate Model for the Ecuadorian territory (RCM-EC), including the mentioned four modeled precipitation datasets in the Reliability Weighted Assembly (REA) (Giorgi and Mearns 2001; Tebaldi and Knutti 2007) approach according to their best ability to reproduce the climatology of Ecuador. The resulting spatial resolution of the RCM-EC is 0.1°, a balance between local climate representation ability and computational power demand to downscale GCMs for the whole country. Since RCM-EC takes advantage of the qualities of several GCMs and is the one that best fits the climatology of Ecuador (Armenta et al. 2016), it is the one that was used in this study to analyze the extremes. However, the downscaled precipitation data from the four GCMs were used to estimate the certainty of the results, both in the bias correction (explained in Section 4.2) and the calculated extremes. In this study, we used data on a daily scale for the historical (1981-2005, 25y) and future (2016-2070, 55y) periods under two Representative Concentration Pathways (RCPs): 4.5 and 8.5. All data was obtained upon request to the MAATE.

4 Methods

Figure 2 shows the methodological sequence followed in this work. The study consisted of four main processes: for the period 1981-2015, the quality control of the training and validation stations was applied, as well as the spatiotemporal distribution of precipitation (RF-MEP model). For 2016-2070, the precipitation projections in the RCP 4.5 and RCP 8.5 scenarios were generated with a bias correction through statistical downscaling. Finally, the last stage included calculating extreme climate indices for the observations and simulations with their respective trend and magnitude analyses. The procedures are detailed below in the following sections.



165 Page 6 of 22 Climatic Change (2024) 177:165

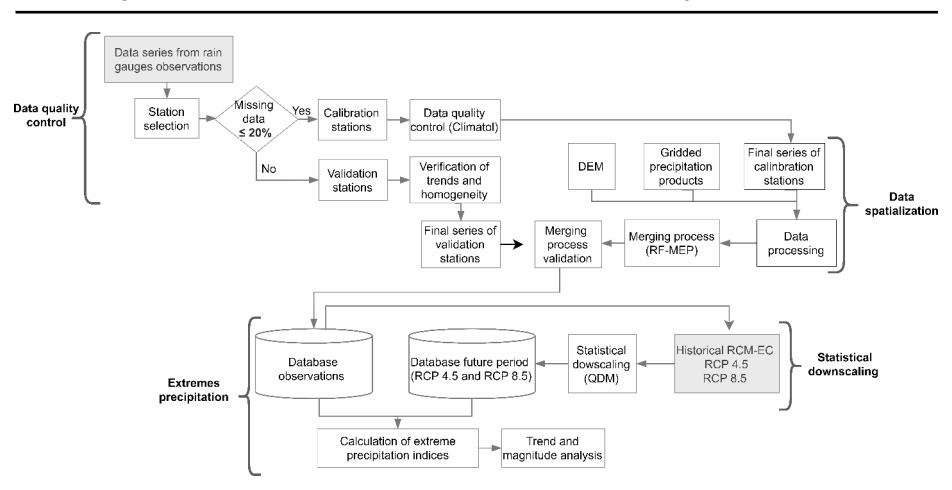


Fig. 2 Methodological outline of the study

4.1 Calibration and validation of gridded precipitation products

The RF-MEP method proposed by Baez-Villanueva et al. (2020) was used to merge gridded precipitation products and rain gauge data to calibrate gridded precipitation estimates. RF-MEP uses a random forest merging procedure, combining gridded precipitation products, ground-based measurements, and other spatial covariates to generate spatially distributed precipitation estimates. The rationality for using this method is based on three assumptions: (1) ground precipitation measurements from rain gauges are accurate at point scale; (2) gridded precipitation products, although prone to bias, still contain valuable information regarding the spatiotemporal pattern of precipitation; and (3) combining multiple gridded precipitation products and ground measurements would yield a better representation of the spatiotemporal variability of precipitation than any individual product. Therefore, gridded precipitation products (i.e., CHIRPS V2.0 and MSWEP V2.2) and in-situ calibration stations generated a reference daily spatial precipitation product for Ecuador from 1981 to 2015. In addition, a Digital Elevation Model (DEM; SRTM v4.1) was used to consider the potential impact of elevation on precipitation. Four different merging combinations were tested to identify the best reference product: (1) CHIRPS V2.0 + rain gauges, (2) MSWEP V2.2 + rain gauges, (3) CHIRPS V2.0 + MSWEP V2.2 + rain gauges, and (4) CHIRPS V2.0 + MSWEP V2.2 + elevation + rain gauges. For a proper comparison of merging products, before the merging procedure, all spatial data were resampled to a common grid cell corresponding to the MSWEP V2.2 product (the coarser grid cell, 0.1°) through the nearest neighbor method. In addition, this spatial resolution is the same as the RCM projections, which supports our selection for the following downscaling procedure. The RF-MEP was executed in R through the Rfmerge v0.1-9 package (Zambrano-Bigiarini et al. 2020), using the default settings for the random forest model. The validation of the performance of the merged products was carried out employing a point-to-pixel comparison with the set of validation stations described in Section 3.2. Three commonly used goodness-of-fit metrics were used to compare the quality of performance of merged products along with the original CHIRPS V2.0 and MSWEP V2.2 products: the mean absolute error (MAE), the root mean



Climatic Change (2024) 177:165 Page 7 of 22 165

square error (RMSE), and the Pearson correlation coefficient (r). The validation procedure was performed in R through the hydroGOF packages (Zambrano-Bigiarini 2017).

4.2 Statistical downscaling

Quantile mapping algorithms are commonly employed to adjust daily precipitation series from climate models, aligning their distributional properties closely with observations (Maraun 2013). Quantile Mapping (QM) has demonstrated exceptional performance in certain hydrological studies when compared to conventional corrections; nevertheless, in studies assessing projected impacts of climate change, simulations may deteriorate and modify the future model projections' trends (Ahmed et al. 2013; Cannon et al. 2015; Tong et al. 2021). Conversely, the Quantile Delta Mapping (QDM) method applied to precipitation preserves the relative changes projected by the model in the quantiles while correcting systematic biases in the quantiles of the modeled series concerning observed values (Cannon et al. 2015). QDM combines two sequential steps: it eliminates the quantile trend from the future model and corrects the bias to the observed data of the calibration period by mapping quantiles. Therefore, the projected relative changes in the quantiles are multiplied by the products of the bias correction model to obtain the results (Cannon et al. 2015). See Cannon et al. (2015) for more details on the method.

Our statistical downscaling model is based on the QDM implementation of the MBC R package (Cannon 2022), which takes into account peculiarities in precipitation data (e.g., the correction of biases in wet day frequency) and other considerations like the computation of empirical quantiles of projected data using a sliding window (Cannon et al. 2015) that other implementations ignore. This method was performed for each pixel of the gridded precipitation area after all spatial data were resampled to a common 0.1° grid using the nearest neighbor method. We used QDM to correct the daily precipitation bias of RCM-EC and the other four downscaled GCMs (i.e., CSIRO-Mk3-6.0, GISS-E2-R, IPSL-CM5A-MR, and MIROC-ESM). To evaluate the downscaling models and estimate how well the models perform in the projections of extreme precipitation indices (detailed in the next section), the historical data were divided into two periods, 1981-1993 and 1994-2005. The period 1981-1993 was used for model calibration. The trained model was then evaluated in the period 1994-2005. The evaluation is based on the one used by Cannon et al. (2015). It considers the proportion of pixels of the gridded precipitation area whose extreme precipitation indices pass the Kolmogorov-Smirnov (KS) test with a 1% significance level. A minor change in the results obtained with the model in the validation period (1994-2005) gives certainty about what is projected for 2016-2070. Once the performance of the models was approximated, the final models were calibrated, leveraging all the available historical data to ensure greater generalization (Raschka and Mirjalili 2019). The latter means that the historical data for the period 1981-2005 (base period) and the observation data (after the spatial distribution of precipitation, see Section 4.1) were used to apply the method and get corrected precipitation projections of two future scenarios, RCP 4.5 and RCP 8.5.

4.3 Extreme precipitation indices

Data from spatially distributed observations and statistically corrected precipitation simulations were used to calculate eleven extreme precipitation indices (Table 1) (ETCCDI 2009).



165 Page 8 of 22 Climatic Change (2024) 177:165

Table 1 Extreme climate indices for precipitation recommended by the ETCCDI

ID	Name	Unit	Description
PRCPTOT	Annual total precipitation on wet days	mm	Precipitation (PRCP) is the sum of wet days (PRCP ≥ 1 mm) for each year.
SDII	Simple Daily Intensity Index	mm/day	The ratio between the precipitation sum of wet days and the number of wet days each year.
R95p	Annual total precipitation on very wet days	mm	Annual precipitation sum of very wet days (PRCP > 95p) for each year. 95p is the 95^{th} percentile of precipitation on wet days (PRCP ≥ 1 mm).
R99p	Annual total precipitation on extremely wet days	mm	Annual precipitation sum of very wet days (PRCP > 99p) for each year. 99p is the 99 th percentile of precipitation on wet days (PRCP ≥ 1 mm).
RX1day	Annual maximum 1-day precipitation	mm	Precipitation on the rainiest day of each year.
RX5day	Annual maximum con- secutive 5-day precipitation	mm	Precipitation of the five consecutive days with the highest accu- mulated precipitation of each year.
CWD	Consecutive wet days	days	The highest number of consecutive wet days (PRCP ≥ 1 mm) of each year.
CDD	Consecutive dry days	days	The highest number of consecutive dry days (PRCP < 1 mm) of each year.
R1mm	Number of wet days	days	Annual count of wet days (PRCP ≥ 1 mm).
R10mm	Number of heavy precipitation days	days	Annual count of days with precipitation ≥ 10 mm.
R20mm	Number of very heavy precipita- tion days	days	Annual count of days with precipitation ≥ 20 mm.

The calculation was done to each of the cells of the spaced data in the historical (1981-2015) and future (2016-2070) periods using our implementation in Python, based on the Climate Library package (Shankar Singh et al. 2023). The indices were grouped according to the different features of precipitation: total precipitation intensity (PRCPTOT and SDII), extreme precipitation intensity (R95p, R99p, RX1day, and RX5day), and precipitation frequency (CWD, CDD, R1mm, R10mm, and R20mm).



Climatic Change (2024) 177:165 Page 9 of 22 165

4.4 Trends and changes

The non-parametric Mann-Kendall test was used to analyze trends in extreme precipitation indices with a significance of 5% (Mann 1945). This test has been widely used in the calculation of trends in hydrometeorological series, as well as in the detection and attribution of trends of extreme climate indices (Subash et al. 2011; Pandey et al. 2021; Islam et al. 2021; Sharma et al. 2022). The null hypothesis H_0 of the test indicates no tendency, and the alternative hypothesis H_1 indicates a monotonous tendency at a certain level of significance (Li et al. 2018). The statistical value S and the statistics of standardized tests Z are calculated with Eq. 1 to apply the Mann-Kendall test.

$$S = \sum_{k=1}^{n_1-1} \sum_{j=k+1}^{n} sgn(x_j - x_k)$$
where: $sgn(x_j - x_k) = \begin{cases} +1 & si & (x_j - x_k) > 0 \\ 0 & si & (x_j - x_k) = 0 \\ -1 & si & (x_j - x_k) < 0 \end{cases}$

$$(1)$$

 x_j y x_k correspond to the values in year j and k, and n is the time series length. The value S has an approximately normal distribution with zero mean and variance represented in Eq. 2 for the estimation of the Z-value Eq. 3:

$$Var(S) = \frac{[(n(n-1)(2n+5)]}{18}$$
 (2)

$$Z = \begin{cases} \frac{S-1}{1} & si & S > 0\\ \frac{(var(S))}{2} & si & S = 0\\ 0 & si & S = 0\\ \frac{S+1}{1} & si & S < 0 \end{cases}$$
(3)

The Z value represents the trend of the time series; if the trend is upward, Z > 0; if the trend is downward, Z < 0 (Li et al. 2018). If the values of Z equal 0, there is no trend (ST). When the values of Z are greater than 1.96, there is a significant increasing trend (TSC). For values of Z less than -1.96, there is a significant decreasing trend (TSD). Furthermore, when the values of Z are between -1.96 and 1.96, there is a non-significant trend (TNS). The values of Z and their corresponding meanings were adapted by Bezerra Alves et al. (2015) and Alencar da Silva Alves and Silva Nóbrega (2017). Trends that were not significant were not ruled out and were analyzed.

On the other hand, Sen's non-parametric method was applied to estimate the trend slope since it is not affected by abrupt data errors or outliers (Karaburun et al. 2011). This method has been used in several studies of the analysis of extreme climatic indices (Karaburun et al. 2011; Cattani et al. 2018; Koubodana et al. 2020; Islam et al. 2021). The Sen test calculates the slope of a trend in the sample of N data pairs using Eq. 4:

$$Q_{i} = \frac{x_{j} - x_{k}}{j - k} \tag{4}$$



Where, $x_j \vee x_k$ are the values corresponding to moments j and k (j > k).

The two non-parametric tests were calculated using the R *trend* package (Pohlert 2023) and applied at the spatial level for observations in the historical period and the projections in the future period.

5 Results

5.1 Gridded precipitation products

Table 2 shows the values of the statistical variables used in the validation process. These statistical tests revealed that merging combinations of gridded precipitation products and ground measurements results in an improved representation of precipitation variability.

The MAE, RMSE, and r values are similar in the merging combinations cases, with an improvement in RMSE and r compared to the precipitation products without combination. On the other hand, the correlation coefficient increases in the merged products, indicating a moderate positive correlation, which is an acceptable value for this research. Similar investigations on precipitation estimation using satellite products in high mountain regions show RMSE values ranging from 4 mm/day to 18 mm/day (Méndez Rivas 2016; Duque Gardeazábal 2018; Liu et al. 2019). Contrary to expectations, in the last fusion case that includes both satellite products, elevation, and rain gauges, the MAE and RMSE values increased slightly. This result suggests that adding the DEM does not provide significant enhancements. The consistent behavior in the analyzed statistical variables allows for the straightforward selection of any of them as a suitable choice for the study. Nevertheless, due to the total availability of the required data in the period of observations (1981-2015) and the ease of use of a single precipitation product, the combination of ground data and the MSWEP V2.2 precipitation product was selected.

5.2 Statistical downscaling

Figure 3 shows the proportion of ETCCDI KS-test passed using the raw RCM data and the QDM-adjusted data in the calibration (Fig. 3a) and validation (Fig. 3b) periods. The performance using the raw data is similar in both periods. In both periods, the results of the CSIRO-Mk3-6-0 model are the ones that best reproduce the extreme indices when the data are not corrected with QDM. On the other hand, the results based on the QDM-corrected data for the calibration period show that, on average, MIROC-ESM better represents the

Table 2 Goodness-of-fit metrics of merged and original CHIRPS V2.0 and MSWEP V2.2 precipitation products

Gridded precipitation products	MAE (mm/day)	RMSE (mm/day)	r
CHIRPS V2.0	6.85	14.42	0.13
MSWEP V2.2	5.83	12.24	0.20
CHIRPS + rain gauges	5.37	10.68	0.40
MSWEP V2.2 + rain gauges	5.36	10.66	0.40
CHIRPS V2.0 + MSWEP V2.2 + rain gauges	5.35	10.63	0.40
CHIRPS V2.0 + MSWEP V2.2 + elevation + rain gauges	5.39	10.70	0.40



Climatic Change (2024) 177:165 Page 11 of 22 165

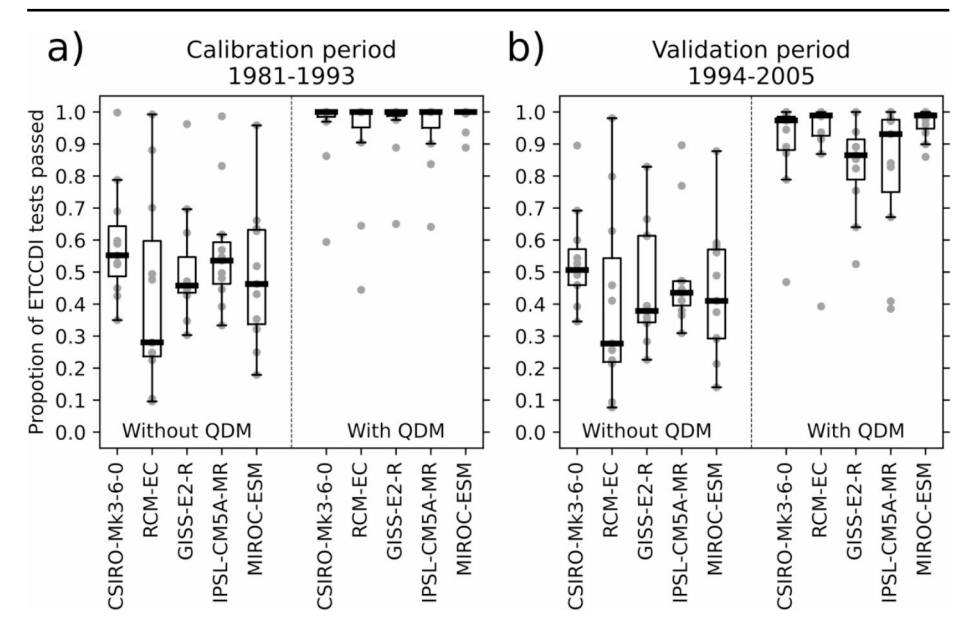


Fig. 3 Distribution over the 11 ETCCDI indices of the proportion of grid cells passing the KS tests in (a) the calibration period (1981-1993) and (b) the validation period (1994-2005)

extremes. However, in the validation period, MIROC-ESM and RCM-EC better reproduce such indices. Although the dispersion increases in the validation period, generally, the average performance is greater than 0.85, which is acceptable for using the models in projections with a sufficient degree of certainty. Specifically, RCM-EC maintains the average and dispersion of performance concerning the calibration period, which is relevant since the interquartile range of RCM-EC in the validation period, but without QDM (Fig. 3b), is slightly lower than that of the calibration period. Due to the above, the results of RCM-EC will be discussed, as it is also the one that is considered the best model in general (Armenta et al. 2016). The results of the rest of the models (i.e., CSIRO-Mk3-6.0, GISS-E2-R, IPSL-CM5A-MR, and MIROC-ESM) will be used to show a band of certainty in the results, both in the historical period and in the projections.

Once the performance was approximated, the models finally used for the rest of the study took advantage of the entire base period data (1981-2005). Applying the statistical down-scaling method allowed us to correct the RCM-EC precipitation projections of the scenarios RCP 4.5 and RCP 8.5, assuming that the statistical features in the historical period remain constant in the future. This bias correction was essential for analyzing future precipitation extremes in regions with complex configurations as the area of study (de Sa Arnal 2017).

5.3 Extreme precipitation indices

Figures S1.1 to S1.9 (Online Resource 1) present the annual times series of the observations and simulations with uncertainty bands by region and the entire country in the historical and future periods of indices: PRCPTOT, SDII, R95p, R99p, RX1day, RX5day, R1mm, R10mm, and R20mm. The uncertainty bands provide a range reflecting the variability and



165 Page 12 of 22 Climatic Change (2024) 177:165

confidence in the results for the historical and future periods. Generally, most indices show significant increasing trends, which are lower in the historical period (where the analyses were carried out with the observations) and higher in the future, especially in the RCP 8.5 scenario.

5.3.1 Total precipitation intensity

PRCPTOT index presents increases in the RCP 4.5 and RCP 8.5 scenarios concerning the historical period, especially in the latter. The Coast region in the historical period shows more significant fluctuations in the time series, with two prominent peaks in 1983 (3011 mm/year) and 1997 (2903 mm/year). The Amazon region recorded the highest annual average value of the historical period (2000 mm), with the same behavior in future scenarios. The Andes region has lower average yearly values than the other two regions. On the other hand, the SDII index presents more significant fluctuations in the Coast region than in other regions. Besides, this region recorded the highest annual average values of 7.87, 8.55, and 8.77 mm/day in the historical period and RCP 4.5 and RCP 8.5 scenarios, respectively. In addition, there was a higher record of precipitation intensity in 1998 in the Coast and Amazon regions, of 12.49 and 7.99 mm/day, respectively.

Figure 4a represents the multi-year average of the PRCPTOT index at the spatial level, showing increases in the index in future periods. Figure 4b presents the index's annual rate variation (slope of the trend line at the yearly scale) at a spatial level. The historical period shows variations that range from 3.43 mm/year to 6.05 mm/year; in the RCP 4.5 scenario, the variation is from 2.06 mm/year to 17.23 mm/year, and in the RCP 8.5 scenario, it is from 2.05 mm/year to 32.82 mm/year. The non-significant trends (NST) prevailed in the historical period.

Figure 4c presents the multi-year average of the SDII index at the spatial level. This index shows a more significant increase in the Coast and Amazon regions. Figure 4d shows the index's annual rate variation; it ranges from -0.026 to 0.03 mm/day in the historical period.

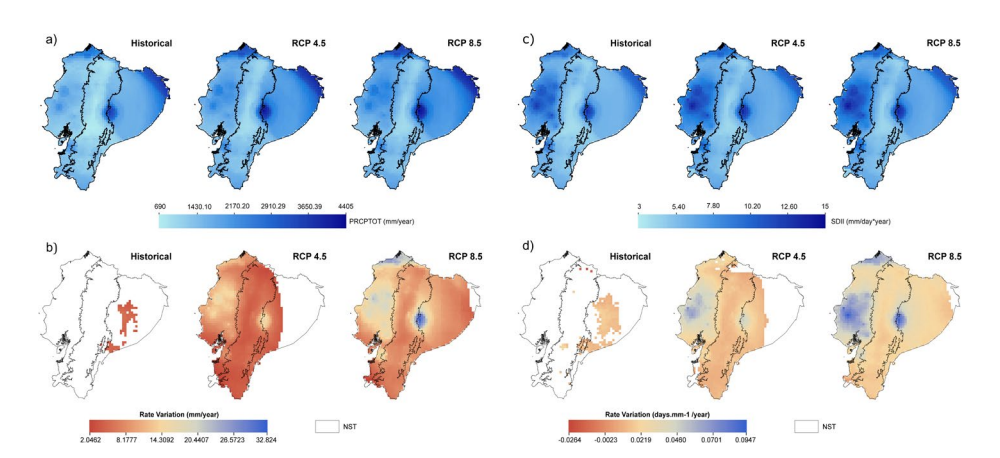


Fig. 4 Multi-year average at the spatial level in the historical and future periods under the projections RCP 4.5 and RCP 8.5 of the indices **a**) PRCPTOT (mm) and **c**) SDII (mm/day); Annual rate variation at the spatial level for the historical period and the future of the projections RCP 4.5 and RCP 8.5 of the indices b) PRCPTOT (mm/year) and d) SDII (mm/day*year). *NST= non-significant trends



Climatic Change (2024) 177:165 Page 13 of 22 165

Besides, this index varies from 0.01 to 0.07 mm/day in the RCP 4.5 scenario. In comparison, the RCP 8.5 scenario presents the index's variations from 0.005 to 0.095 mm/day.

5.3.2 The intensity of extreme precipitation

The annual average of the R95p index in the Amazon region in the historical period is 365.61 mm, slightly above the annual average value of the Coast region (351.40 mm). However, the Coast region presents the most significant fluctuations in the historical and future projections, with a maximum peak recorded in 1998 of 1245.47 mm. In the RCP 4.5 and RCP 8.5 projections, the Coast region has the highest annual average, followed by the Amazon region. In contrast, the Andes region has a lower yearly average than these regions. On the other hand, the R99p index has a similar behavior to the R95 index. The Coast region evidenced two maximum peaks in 1983 and 1998, 294.05 and 534.96 mm, respectively. However, the Amazon region registered the highest annual average in the historical period (102.38 mm) compared to the other two regions. In the projections RCP 4.5 and RCP 8.5, there are increases in the annual average values, evidencing more significant fluctuations in the Coast and Amazon region.

Figure 5a and c show the spatial level's multi-year average of the R95p and R99p indices, respectively. Both present increases in future periods concerning the historical period; the highest incidence is recorded in the Coast and Amazon regions. On the other hand, Fig. 5b shows the spatial distribution of the annual rate variation of the R95p index. This index ranges from -4.53 to 7.01 mm/year in the historical period, and the future scenarios, it ranges from 1.32 to 9.89 mm/year and from 2.18 to 16.78 mm/year for the RCP 4.5 and RCP 8.5, respectively. The annual rate variation of the R99p index (Fig. 5d) in the historical period fluctuates from -2.39 to 3.70 mm/year; in the RCP 4.5 scenario, it varies from 0.51 to 3.73 mm/year, and in the RCP 8.5 scenario varies from 0.72 to 5.70 mm/year.

The RX1day index in the Coast region registered the highest annual averages for the historical period, RCP 4.5 and RCP 8.5, which present values of 51.80, 58.58, and 61.19 mm, respectively. In addition, the maximum peaks in the Coast region's historical period

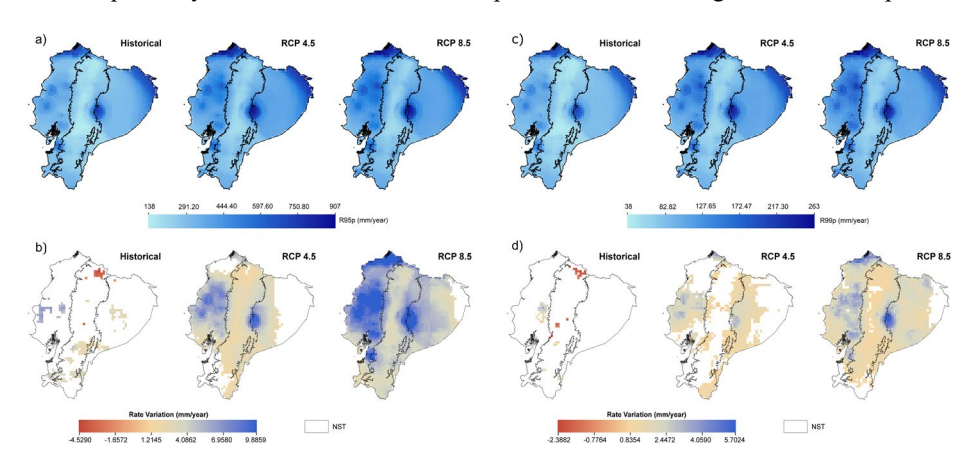


Fig. 5 Multi-year average at the spatial level in the historical and future periods under the projections RCP 4.5 and RCP 8.5 of the indices **a**) R95p (mm) and **c**) R99p (mm); Annual rate variation at the spatial level for the historical period and the future of the projections RCP 4.5 and RCP 8.5 of the indices **b**) R95p (mm/year) and **d**) R99p (mm/year). *NST= non-significant trends



165 Page 14 of 22 Climatic Change (2024) 177:165

occurred in 1983 and 1998, with values of 67.39 and 76.07 mm, respectively. On the other hand, the annual averages of the RX5day index display similar patterns. The Coast region presents the highest average values concerning the other regions, with average values of 122.21, 155.81, and 163.60 mm for the historical period and RCP 4.5 and RCP 8.5 projections, respectively. On the other hand, the Andes region presents lower average values than the Coast and Amazon regions. Figure 6a and c show the spatial level's multi-year average of the RX1day and RX5day indices over the historical period and RCP 4.5 and RCP 8.5 projections. These figures highlight an increase in these indices under the RCP 8.5 scenario.

On the other hand, Fig. 6b shows the spatial distribution of the annual rate variation of the RX1day index, which ranges from -0.35 to 0.83 mm/year for the historic period. This index varies between 0.05 and 0.64 mm/year and 0.03 to 0.59 mm/year in the RCP 4.5 and RCP 8.5 scenarios. Similarly, Fig. 6d shows the spatial distribution of the annual rate variation of the RX5day index. This index fluctuates between -0.82 to 0.44 mm/year in the historical period. Moreover, this index presents variations from 0.24 to 1.43 mm/year in RCP 4.5 and from 0.19 to 1.85 mm/year in the RCP 8.5 scenario.

5.3.3 Precipitation frequencies

The R1mm index shows low fluctuations across the regions, with an average value of 289.48 days of precipitation exceeding 1 mm in the Amazon region, followed by the Andes region with a value of 233.07 days. In the future scenarios RCP4.5 and RCP8.5, the values increase. The annual average of the R10mm index in the historical period in the Amazon is 61.36 days, which was higher compared to the other regions; meanwhile, in this region, annual averages of 74.18 and 78.28 days are expected in the scenarios RCP 4.5 and RCP 8.5, respectively. Some notable highs in the yearly series are 102.70 days in the Coast region in 1983 and 82.74 days in the Amazon in 1999. On the other hand, the highest annual average of the R20mm index is 7.74 days in the Coast region, with more significant increases in the scenarios RCP 4.5 and RCP 8.5 of 23.33 and 25.05 days, respectively. In the same future scenarios, the Amazon region presents annual averages of 18.32 and 19.75 days. Likewise,

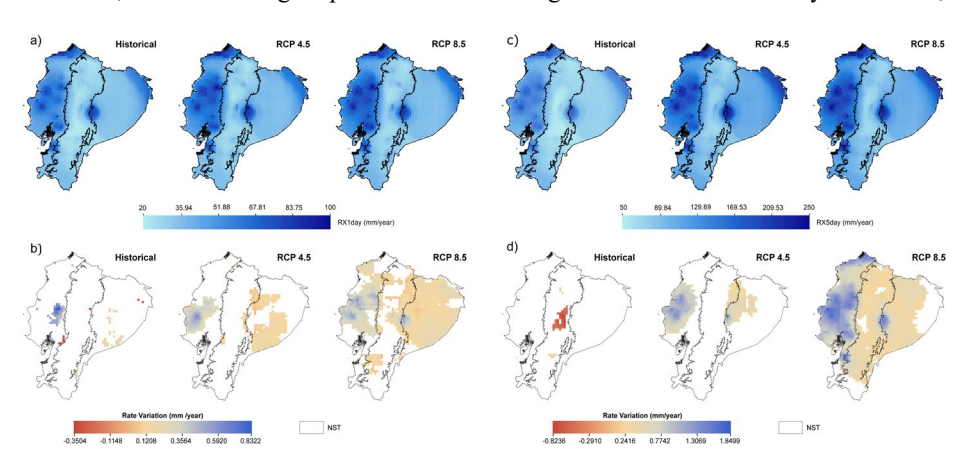


Fig. 6 Multi-year average at the spatial level in the historical and future periods under the projections RCP 4.5 and RCP 8.5 of the indices **a**) RX1day (mm) and **c**) RX5day (mm); Annual rate variation at the spatial level for the historical period and the future of the projections RCP 4.5 and RCP 8.5 of the indices **b**) RX1day (mm/year) and **d**) RX5day (mm/year). *NST= non-significant trends



Climatic Change (2024) 177:165 Page 15 of 22 165

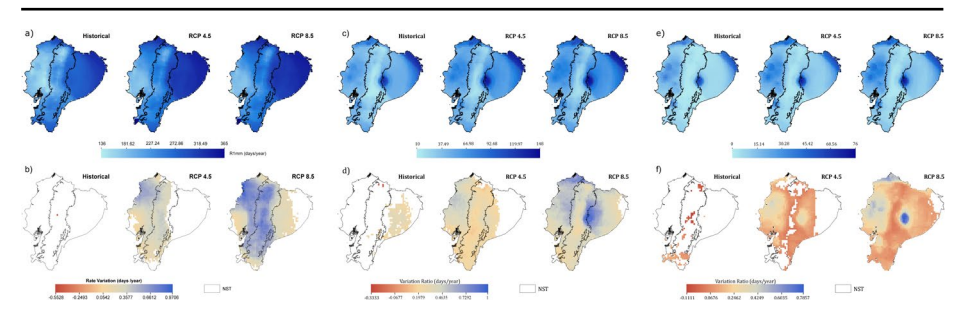


Fig. 7 Multi-year average at the spatial level in the historical and future periods under the projections RCP 4.5 and RCP 8.5 of the indices **a**) R1mm (days),**c**) R10mm (days) and **e**) R20mm (days); Annual rate variation at the spatial level for the historical period and the future of the projections RCP 4.5 and RCP 8.5 of the indices **b**) R1mm (days/year), **d**) R10mm (days/year) and f) R20mm (days/year). *NST= non-significant trends

Table 3 Percentage of the area with significant increasing trends

	RCP4.5			RCP8.5		
	Coast	Andes	Amazon	Coast	Andes	Amazon
PRCPTOT	97.5	99.0	34.1	99.2	100.0	93.6
SDII	93.5	95.7	43.5	99.2	100.0	94.2
R95p	76.3	87.1	47.5	99.7	100.0	86.6
R99p	47.3	35.3	48.3	91.9	87.1	83.4
RX1day	24.04	6.6	35.1	54.5	36.6	83.0
RX5day	35.4	6.6	18.8	90.8	83.9	73.8
R1mm	86.2	75.1	6.6	93.2	97.9	61.7
R10mm	93.2	95.6	35.2	97.3	99.9	91.5
R20mm	80.1	64.7	44	100.0	99.9	86.8

maximum peaks in the Coast region were present in 1983 and 1998, with 42.79 and 46.50 days, respectively. Figure 7 shows the spatial level's multi-year average of the R1mm (Fig. 7a), R10mm (Fig. 7c), and R20mm (Fig. 7e) indices in the historical period and RCP 4.5 and RCP 8.5 projections. In the future, these indices will significantly increase in the north and center of the Amazon region and the north of the Coast.

Figure 7b shows the spatial distribution of the annual rate variation of the R1mm index. The annual variation of the R1mm index in the historical period is -0.55 days/year; in the RCP 4.5 scenario, it ranges from 0.04 to 0.68 days/year, and in the RCP 8.5 scenario, it varies from 0 to 0.97 days/year. Figure 7d shows the spatial distribution of the annual rate variation of the R10mm index. This index varies from -0.33 to 0.47 days/year in the historical period. In the RCP 4.5, R10mm fluctuates between 0.12 and 0.57 days/year; in the RCP 8.5, it ranges from 0.17 to 1 day/year. In comparison, Fig. 7f shows the spatial distribution of the annual rate variation of the R20mm index. This index ranges from -0.11 to 0.17 days/year in the historical period. In the RCP 4.5 and RCP 8.5 scenarios, the R20mm index varies from 0 to 0.45 days/year and from 0.02 to 0.79 days/year, respectively.

Table 3 provides a summary of the percentage of the area with significant increasing trends calculated for each region in the future periods under the projections RCP 4.5 and RCP 8.5 of indices: PRCPTOT, SDII, R95p, R99p, RX1day, RX5day, R1mm, R10mm, and R20mm. The CWD and CDD indices present abrupt jumps from historical to future periods



165 Page 16 of 22 Climatic Change (2024) 177:165

and atypical temporal and spatial behaviors. These results are discussed in Online Resource 2.

6 Discussion and conclusions

The present study found that applying bias correction using the QDM method improved the RCM-EC model and the baseline models from which the latter originates. These findings suggest that reliance on specific models without adequate correction can lead to misinterpretations of climatic extremes. Therefore, their limitations must be considered, as regional climate projections or models carry uncertainties related to spatial resolution and the ability to represent the climate system. Consequently, the results cannot be assumed to be predictions but are possible future climate states, so they should be interpreted cautiously (Armenta 2016; Shrestha and Roachanakanan 2021). Applying the statistical downscaling method was crucial for correcting precipitation projections under RCP 4.5 and RCP 8.5 scenarios. The results demonstrate that the average performance exceeds 85% during the validation period, which is deemed acceptable for utilizing the models to evaluate the extreme precipitation projections with reduced uncertainty (Fauzi et al. 2020; Freitas Xavier et al. 2022).

The application of extreme precipitation indices allowed the analysis of events and their historical and future climatic trends in the continental Ecuadorian territory. Concerning uncertainty bands, most indices exhibit narrow bands, suggesting lower uncertainty in the projections. However, in the Coastal region, specifically in the RX1day and RX5day indices, broad bands are observed under the RCP 4.5 and RCP 8.5 scenarios. Previous studies have revealed higher percentage increases in these indices than others, such as PRCPTOT and SDII, indicating disproportionately larger increments (Sillmann et al. 2013; Zhou et al. 2014). This fact could be attributed to their greater sensitivity to temperature than other indices (Avila-Diaz et al. 2021) due to the intensification of daily precipitation by convective processes based on increased heat and water vapor (Bengtsson 2010). On the other hand, it may also be related to regional climate variability, which climate models do not capture equally, and differences in forcing scenarios (Zhou et al. 2014), all of which contribute to uncertainty in the projections.

In the historical period (analyzing the observations), the Coast region presented the most significant increases in magnitude in 1983 and 1998 in the PRCPTOT, SDII, R99p, RX1day, RX5day, R1mm, and R20mm indices (Online Resource 1). These indices indicate conditions of maximum precipitation. There is evidence that in the periods of 1982-1983 and 1997-1998, as a result of the presence of the El Niño phenomenon, continuous, considerable, and long-lasting precipitation of more than 30 h was recorded, with particular affection to the Coast (Zuleta and Arauz Calderón 1998; Thielen et al. 2016). Likewise, in their study, Morán Tejeda et al. (2016) found that in the coastal region, there is a close relationship between the magnitude and seasonal distribution of precipitation and the variability of El Niño 1+2. The analyses showed between 1966 and 2011 a stationary evolution with two peaks in 1983 and 1997 (extreme El Niño events). On the other hand, in the historical analysis of the observations by regions (Coast, Andes, and Amazon) in the indices analyzed (PRCPTOT, SDII, R1mm, R10mm, R20mm, R95p, and R99p), a decrease in precipitation was found in 1985 (Online Resource 1). These results could be attributed to the fact that there are more prolonged rainless seasons in Ecuador, especially over a considerable sec-



Climatic Change (2024) 177:165 Page 17 of 22 165

tion of the Coast and Andean territory, with long dry days (Ministry of Environment Water and Ecological and Transition 2021). Similarly, Vicente Serrano et al. (2017) in their study mentioned that from 1985 to 2000, drought events have been more frequent in the country. Regarding the future projections of the RCP 4.5 and RCP 8.5 scenarios, all the indices evaluated showed higher increases, especially for the RCP 8.5 scenario.

Concerning the trends of the extreme indices in the historical period 1981-2015 (analyzing the observations), non-significant trends were found in the PRCPTOT, SDII, R95p, R99p, RX1day, RX5day, R1mm, R10mm, and R20mm indices; however, the Amazon region showed significant trends in all indices, being the largest in the R10mm index, with a cover of 42%. In the RCP 4.5 scenario in the Coast and Andes regions, significant increasing trends prevailed in the PRCPTOT, SDII, R95p, R1mm, R10mm, and R20mm indices. However, the Amazon region presented a lower percentage of these indices' significant trends than the other regions. In this same scenario, the R99p, RX1day, and RX5day indices showed a predominance of non-significant trends. On the other hand, in the RCP 8.5 scenario, a higher percentage was recorded in the increases of the significant increasing trends in all regions in the PRCPTOT, SDII, R95p, R99p, RX1day, RX5day, R1mm, R10mm, and R20mm indices. The trends analyzed in the indices show similar patterns in some areas studied, with greater incidence in the Coast region. In general, all indices foresee increases corresponding to wetter conditions in the future. The results are consistent with the study by Haylock et al. (2006), in a similar historical period, reported that the trends of the PRCP-TOT index indicate wetter conditions in Ecuador and northwestern Peru. Likewise, Castillo et al. (2018) detail that both scenarios cause changes in the climatic conditions of Central America, the Caribbean, and the Pacific regions, generating wetter systems in Ecuador, Peru, and Colombia. The IPCC has generally detailed the possibility of increasing extreme precipitation's intensity and frequency in future scenarios (Field et al. 2012). Besides, it would present an increase in unfamiliar precipitation patterns with a high confidence level (IPCC AR6 2022).

In continental Ecuador, studies have been carried out on climate variability, analysis of extreme precipitation indices, and evaluation of droughts in the RCP 4.5 and RCP 8.5 scenarios. In the southern Andes, precisely in the upper basin of the Paute River, Zhiña et al. (2019) studied droughts with long-term future spatiotemporal projections (2011-2070). They found a decreasing pattern in drought severity for scenarios RCP 4.5 and RCP 8.5 and a drastic decrease in the durations and magnitudes of droughts in future scenarios. Similarly, Campozano et al. (2020) mention the presence of a slightly decreasing trend in future droughts throughout the country, with the most significant decrease in moderate droughts, followed by severe and extreme droughts for the RCP 4.5 and RCP 8.5 scenarios. On the other hand, in investigating trends and extreme climatic events for the historical period 2000-2015, Armenta (2016) found fewer consecutive dry days in the country. Besides, wet and highly humid days increased in the north-central and southern parts of the Andes and specific sectors of the Amazon. The findings of these studies suggest a decrease in droughts and an increase in precipitation, which is consistent with the results found in the present research.

In calculating the CWD and CDD indices for the RCP 4.5 and RCP 8.5 projections, inconsistencies related to outliers and the extreme precipitation indices patterns were detected. These may be related to the inability and limitations of the climate models (GCMs/RCMs) to represent certain phenomena. In addition, several uncertainties still need to be



165 Page 18 of 22 Climatic Change (2024) 177:165

addressed for analyzing extreme events, such as incrementing ground gauge data (especially in the Amazon region), testing new regional climate modeling experiments and downscaling methods, and alternative future scenarios.

Finally, calculating and analyzing extreme precipitation indices could direct adaptation actions and strategies in the coming years. However, the impacts of extreme climate events on health, agriculture, and water resource management remain to be explored, so additional research efforts should be directed in this way.

Supplementary Information The online version contains supplementary material available at https://doi.org/10.1007/s10584-024-03820-4.

Acknowledgements The authors thank the Dirección de Vinculación y Vicerrectorado de Investigación de la Universidad de Cuenca, for the support provided to the project "Seguridad Hídrica de la subcuenca del río Tabacay en tiempos de cambios globales". We thank the National Institute of Meteorology and Hydrology (INAMHI) and the Ministry of Environment, Water and Ecological Transition (MAATE) for providing the climate data used in this work. Many thanks to Ana Loja for his support in the manuscript writing revision. A.V.-P. acknowledges to the VIUC for supporting him through "Conjunto de horas 1".

Author contributions Conceptualization: [Katy Valdivieso-García, Hugo Saritama, Alex Avilés]; Data curation: [Katy Valdivieso-García, Hugo Saritama, Angel Vázquez-Patiño]; Methodology: [Katy Valdivieso-García, Hugo Saritama, Juan Contreras, Alex Avilés, Angel Vázquez-Patiño]; Formal analysis and investigation: [Katy Valdivieso-García, Hugo Saritama, Juan Contreras]; Writing - original draft preparation: [Katy Valdivieso-García, Hugo Saritama]; Writing - review and editing: [Katy Valdivieso-García, Hugo Saritama, Juan Contreras, Alex Avilés, Fernando García, Angel Vázquez-Patiño]; Resources: [Alex Avilés, Fernando García]; Supervision: [Alex Avilés].

Funding No funding was received for conducting this study.

Data availability The datasets used in the current study are not publicly available and must be requested to the INAMHI and MAATE.

Code availability Code used in the current study is available upon reasonable request to the corresponding author.

Declarations

Ethics approval Not applicable.

Consent for publication Not applicable.

Competing interests There is no competing interest concerning the study.

References

Ahmed KF, Wang G, Silander J et al (2013) Statistical downscaling and bias correction of climate model outputs for climate change impact assessment in the U.S. northeast. Glob Planet Change 100:320–332. https://doi.org/10.1016/J.GLOPLACHA.2012.11.003

Alencar da Silva Alves KM, Silva Nóbrega R (2017) Tendencia pluviométrica y concentración estacional de precipitación en la cuenca hidrográfica del río Moxotó-Pernamcuco-Brasil. Rev Geográfica América Cent 1:295. https://doi.org/10.15359/RGAC.58-1.12



Climatic Change (2024) 177:165 Page 19 of 22 165

Alexander L, Tebaldi C (2012) Climate and weather extremes: observations, modelling, and projections. In: Henderson-Sellers A, McGuffie K (eds) The future of the world's climate, 2nd edn. Elsevier, Boston, pp 253–288

- Armenta GE (2016) Análisis de tendencias climáticas y eventos climáticos extremos para Ecuador. Ecuador Armenta G, Villa J, Jácome PS (2016) Proyecciones climáticas de precipitación y temperatura para Ecuador, bajo distintos escenarios de cambio climático. Ouito Ecuador
- Avila-Diaz A, Bromwich DH, Wilson AB et al (2021) Climate extremes across the North American Arctic in modern reanalyses. J Clim 34:2385–2410. https://doi.org/10.1175/JCLI-D-20-0093.1
- Baez-Villanueva OM, Zambrano-Bigiarini M, Ribbe L et al (2018) Temporal and spatial evaluation of satellite rainfall estimates over different regions in Latin-America. Atmos Res 213:34–50. https://doi.org/1 0.1016/j.atmosres.2018.05.011
- Baez-Villanueva OM, Zambrano-Bigiarini M, Beck HE et al (2020) RF-MEP: a novel random forest method for merging gridded precipitation products and ground-based measurements. Remote Sens Environ 239:111606. https://doi.org/10.1016/j.rse.2019.111606
- Ballari D, Giraldo R, Campozano L, Samaniego E (2018) Spatial functional data analysis for regionalizing precipitation seasonality and intensity in a sparsely monitored region: unveiling the spatio-temporal dependencies of precipitation in Ecuador. Int J Climatol 38:3337–3354. https://doi.org/10.1002/joc.5 504
- Beck HE, Wood EF, Pan M et al (2019) MSWep v2 global 3-hourly 0.1° precipitation: methodology and quantitative assessment. Bull Am Meteorol Soc 100:473–500. https://doi.org/10.1175/BAMS-D-17-0138.1
- Bezerra Alves TL, Vieira de Azevedo P, de Farias AA (2015) Rainfall behavior rain and its relationship with relief in the Regions Cariri of Eastern and Western state of Paraíba. Rev Bras Geogr Física 8:1601–1614. https://doi.org/10.5935/1984-2295.20150090
- Campozano L, Célleri R, Trachte K et al (2016) Rainfall and cloud dynamics in the Andes: a Southern Ecuador case study. Adv Meteorol. https://doi.org/10.1155/2016/3192765
- Campozano L, Ballari D, Montenegro M, Avilés A (2020) Future meteorological droughts in Ecuador: decreasing trends and associated spatio-temporal features derived from CMIP5 models. Front Earth Sci. https://doi.org/10.3389/feart.2020.00017
- Cannon AJ (2022) Multivariate bias correction of climate model outputs MBC R Package. R Packag. MBC 17
- Cannon AJ, Sobie SR, Murdock TQ (2015) Bias correction of GCM precipitation by quantile mapping: how well do methods preserve changes in quantiles and extremes? J Clim 28:6938–6959. https://doi.org/10.1175/JCLI-D-14-00754.1
- Castillo R, Montero R, Amador J, Durán AM (2018) Cambios futuros de precipitación y temperatura sobre América Central y el Caribe utilizando proyecciones climáticas de reducción de escala estadística. Rev Climatol 18:1–2
- Cattani E, Merino A, Guijarro JA, Levizzani V (2018) East Africa rainfall trends and variability 1983–2015 using three long-term Satellite products. Remote Sens 10:931. https://doi.org/10.3390/RS10060931
- Cuartas DE, Caicedo DM, Ortega D et al (2017) Tendencia espacial y temporal de eventos climáticos extremos en el valle Geográfico del Río Cauca| Revista U.D.C.A Actualidad & Divulgación Científica. Rev UDCA Actual Divulg
- de Sa Arnal BA (2017) Proyecciones climáticas de índices extremos par El Periodo 2021-2050 en la España Peninsular. Universidad de Vigo
- Duque Gardeazábal N (2018) Estimación de campos de precipitación en cuencas hidrográficas colombianas con escasez de datos, combinando datos teledetectados y de estaciones en tierra, utilizando funciones de Kernel. Universidad Nacional de Colombia
- Esquivel A, Llanos-Herrera L, Agudelo D et al (2018) Predictability of seasonal precipitation across major crop growing areas in Colombia. Clim Serv 12:36–47. https://doi.org/10.1016/j.cliser.2018.09.001
- ETCCDI (2009) Climate Change Indices. In: CLIVAR-WCP. http://etccdi.pacificclimate.org/list_27_indic es.shtml
- Fauzi F, Kuswanto H, Atok RM (2020) Bias correction and statistical downscaling of earth system models using quantile delta mapping (QDM) and bias correction constructed analogues with quantile mapping reordering (BCCAQ). J Phys Conf Ser doi. https://doi.org/10.1088/1742-6596/1538/1/012050
- Fernandez-Palomino CA, Hattermann FF, Krysanova V et al (2022) A novel high-resolution gridded precipitation dataset for Peruvian and Ecuadorian watersheds: development and hydrological evaluation. J Hydrometeorol 23:309–336. https://doi.org/10.1175/JHM-D-20-0285.1
- Field CB, Barros V, Stocker TF et al (2012) Managing the risks of extreme events and disasters to advance climate change adaptation special, Cambridge. Cambridge, UK



165 Page 20 of 22 Climatic Change (2024) 177:165

Freitas Xavier AC, Lopes Martins L, Rudke AP et al (2022) Evaluation of quantile delta mapping as a biascorrection method in maximum rainfall dataset from downscaled models in São Paulo state (Brazil). Int J Climatol 42:175–190. https://doi.org/10.1002/joc.7238

- Funk C, Peterson P, Landsfeld M et al (2015) The climate hazards infrared precipitation with stations—a new environmental record for monitoring extremes. Sci Data 2:150066. https://doi.org/10.1038/sdata.2015.
- Gentilucci M, Barbieri M, D'Aprile F, Zardi D (2020) Analysis of extreme precipitation indices in the Marche region (central Italy), combined with the assessment of energy implications and hydrogeological risk. Energy Rep 6:804–810. https://doi.org/10.1016/j.egyr.2019.11.006
- Giorgi F, Mearns LO (2001) Calculation of average, uncertainty range and reliability of regional climate changes from AOGCM simulations via the reliability ensemble averaging (REA) method. J Clim 15:1141–1157
- Guijarro JA (2018) Homogeneización de series climáticas con Climatol. España
- Haylock MR, Peterson TC, Alves LM et al (2006) Trends in total and extreme south American rainfall in 1960-2000 and links with sea surface temperature. J Clim 19:1490–1512
- Ilbay-Yupa M, Lavado-Casimiro W, Rau P et al (2021) Updating regionalization of precipitation in Ecuador. Theor Appl Climatol 143:1513–1528. https://doi.org/10.1007/s00704-020-03476-x
- IPCC AR6, H.-O. Pörtner, D.C. Roberts, M. Tignor, E.S. Poloczanska, K. Mintenbeck, A. Alegría, M. Craig, S. Langsdorf, S. Löschke, V. Möller, A. Okem, B. Rama (eds.) (2022) Technical Summary In: Climate Change 2022: Impacts, Adaptation and Vulnerability. Cambridge University Press, UK and NY, USA
- Islam HMT, Islam ARMT, Abdullah-Al-Mahbub M et al (2021) Spatiotemporal changes and modulations of extreme climatic indices in monsoon-dominated climate region linkage with large-scale atmospheric oscillation. Atmos Res 264:105840. https://doi.org/10.1016/J.ATMOSRES.2021.105840
- Karaburun A, Demirci A, Fatih K (2011) Analysis of spatially distributed annual, seasonal and monthly temperatures in Istanbul from 1975 to 2006. World Appl Sci J 12:1662–1675
- Karl TR, Nicholls N, Ghazi A (1999) CLIVAR/GCOS/WMO workshop on indices and indicators for climate extremes workshop summary. In: Karl TR, Nicholls N, Ghazi A (eds) Weather and climate extremes: changes, variations and a perspective from the Insurance Industry. Springer Netherlands, Dordrecht, pp 3–7
- Kinouchi T, Nakajima T, Mendoza J et al (2019) Water security in high mountain cities of the Andes under a growing population and climate change: a case study of La Paz and El Alto, Bolivia. Water Secur 6:100025. https://doi.org/10.1016/j.wasec.2019.100025
- Koubodana HD, Adounkpe J, Tall M et al (2020) Trend analysis of hydro-climatic historical data and future scenarios of climate extreme indices over Mono River Basin in West Africa. Am J Rural Dev 8:37–52. https://doi.org/10.12691/AJRD-8-1-5
- Leng G, Tang Q, Rayburg S (2015) Climate change impacts on meteorological, agricultural and hydrological droughts in China. Glob Planet Change 126:23–34. https://doi.org/10.1016/j.gloplacha.2015.01.003
- Li M, Chu R, Shen S, Islam ARMT (2018) Dynamic analysis of pan evaporation variations in the Huai River Basin, a climate transition zone in eastern China. Sci Total Environ 625:496–509. https://doi.org/10.1016/J.SCITOTENV.2017.12.317
- Liu J, Shangguan D, Liu S et al (2019) Evaluation and comparison of CHIRPS and MSWEP daily-precipitation products in the Qinghai-Tibet Plateau during the period of 1981–2015. Atmos Res 230:104634. https://doi.org/10.1016/J.ATMOSRES.2019.104634
- MAE-PNUD (2017) Tercera Comunicación Nacional del Ecuador a la Convención Marco de las Naciones Unidas sobre Cambio Climático. Ministerio de Ambiente y Agua, Quito Ecuador
- Mann HB (1945) Non-parametric test against Trend. Econometrica 13:245-259
- Maraun D (2013) Bias correction, quantile mapping, and downscaling: revisiting the inflation issue. J Clim 26:2137–2143. https://doi.org/10.1175/JCLI-D-12-00821.1
- Méndez Rivas RA (2016) Productos de precipitación satelital de alta resolución espacial y temporal en zonas de topografía compleja. Pontificia Universidad Católica de Chile
- Milanovic M, Gocic M, Trajkovic S (2015) Analysis of extreme climatic indices in the area of Nis and Belgrade for the period between 1974 and 2003. Agric Agric Sci Procedia 4:408–415. https://doi.org/10.1016/j.aaspro.2015.03.046
- Ministry of Environment Water and Ecological Transition M (2021) Ecuador drought plan 2021-2025. Quito Montenegro M, Mendoza D, Mora D et al (2022) Extreme rainfall variations under climate change scenarios. Case of study in an Andean Tropical River Basin. Water Resour Manag 36:5931–5944. https://doi.org/10.1007/s11269-022-03332-9
- Morán Tejeda E, Bazo J, López-Moreno JI et al (2016) Climate trends and variability in Ecuador (1966–2011). Int J Climatol 36:3839–3855. https://doi.org/10.1002/joc.4597
- Palmer TN, Räisänen J (2002) Quantifying the risk of extreme seasonal precipitation events in a changing climate. Nature 415:512–514. https://doi.org/10.1038/415512a



Climatic Change (2024) 177:165 Page 21 of 22 165

Pandey VP, Shrestha D, Adhikari M (2021) Characterizing natural drivers of water-induced disasters in a rain-fed watershed: hydro-climatic extremes in the extended East Rapti Watershed, Nepal. J Hydrol 598:126383. https://doi.org/10.1016/J.JHYDROL.2021.126383

- Peterson T, Folland C, Hogg W et al (2001) Report on the activities of the working group on climate change detection and related rapporteurs. World Meteorological Organization, Geneva
- Pohlert T (2023) Non-parametric trend tests and change-point detection trend R Package. 38
- Raschka S, Mirjalili V (2019) Python machine learning: machine learning and deep learning with Python, scikit-learn, and TensorFlow 2, 2nd edn
- Scholze M (2014) El Cambio Climático en la Región Amazónica. Organización del Tratado de Cooperación Amazónica (OTCA), Brasilia
- Serrano Vincenti S, Zuleta D, Moscoso V et al (2012) Análisis estadístico de datos meteorológicos mensuales y diarios para la determinación de variabilidad climática y cambio climático en el Distrito Metropolitano de Quito. La Granja 16:23–47. https://doi.org/10.17163/lgr.n16.2012.03
- Serrano Vincenti S, Reisancho Puetate A, Borbor Córdova MJ, Stewart Ibarra AM (2016) Análisis de inundaciones costeras por precipitaciones intensas, cambio climático y fenómeno de El Niño. Caso de estudio: Machala. La Granja Rev Ciencias La Vida 24:53–68
- Shankar Singh S, Nanda A, Attada R (2023) A python library for climate indices climate-library (v1.0.0). Clim. Libr
- Sharma A, Sharma D, Panda SK (2022) Assessment of spatiotemporal trend of precipitation indices and meteorological drought characteristics in the Mahi River basin, India. J Hydrol 605:127314. https://doi.org/10.1016/J.JHYDROL.2021.127314
- Shrestha S, Roachanakanan R (2021) Extreme climate projections under representative concentration pathways in the Lower Songkhram River Basin. Thail Heliyon 7:e06146. https://doi.org/10.1016/J.HELIY ON.2021.E06146
- Sillmann J, Kharin VV, Zwiers FW et al (2013) Climate extremes indices in the CMIP5 multimodel ensemble: part 2. Future climate projections. J Geophys Res Atmos 118:2473–2493. https://doi.org/10.1002/jgrd.50188
- Sisco MR, Bosetti V, Weber EU (2017) When do extreme weather events generate attention to climate change? Clim Change 143:227–241. https://doi.org/10.1007/s10584-017-1984-2
- Subash N, Singh SS, Priya N (2011) Extreme rainfall indices and its impact on rice productivity—a case study over sub-humid climatic environment. Agric Water Manag 98:1373–1387. https://doi.org/10.1016/J.AGWAT.2011.04.003
- Tebaldi C, Knutti R (2007) The use of the multi-model ensemble in probabilistic climate projections. Philos Trans R Soc Math Phys Eng Sci 365:2053–2075. https://doi.org/10.1098/rsta.2007.2076
- Thielen D, Cevallos J, Erazo T et al (2016) Dinámica espacio-temporal de las precipitaciones durante el evento de El Niño 97/98 en la cuenca de Río Portoviejo, Manabí, costa ecuatoriana del Pacífico. Rev Climatol 16:35–50
- Thielen DR, Ramoni-Perazzi P, Puche ML et al (2023) Effect of extreme El Niño events on the precipitations of Ecuador. Nat Hazards Earth Syst Sci 23:1507–1527. https://doi.org/10.5194/nhess-23-1507-2023
- Tobar V, Wyseure G (2018) Seasonal rainfall patterns classification, relationship to ENSO and rainfall trends in Ecuador. Int J Climatol 38:1808–1819. https://doi.org/10.1002/joc.5297
- Tong Y, Gao X, Han Z et al (2021) Bias correction of temperature and precipitation over China for RCM simulations using the QM and QDM methods. Clim Dyn 57:1425–1443. https://doi.org/10.1007/S00382-020-05447-4/FIGURES/10
- Torres Pineda CE, Pabón Caicedo JD (2017) Variabilidad intraestacional de la precipitación en Colombia y su relación con la oscilación de Madden-Julian. Rev Acad Colomb Ciencias Exactas Físicas Nat 41(158):79
- Touré Halimatou A, Kalifa T, Kyei Baffour N (2017) Assessment of changing trends of daily precipitation and temperature extremes in Bamako and Ségou in Mali from 1961- 2014. Weather Clim Extrem 18:8–16. https://doi.org/10.1016/j.wace.2017.09.002
- Ulloa J, Ballari D, Campozano L, Samaniego E (2017) Two-step downscaling of Trmm 3b43 V7 precipitation in contrasting climatic regions with sparse monitoring: the case of Ecuador in Tropical South America. Remote Sens 9:758. https://doi.org/10.3390/rs9070758
- Uribe E (2017) El cambio climático y sus efectos en la biodiversidad de América Latina
- Useros JL (2013) El Cambio climático: sus causas y efectos medioambientales. Anales de La Real Acad Med Y Cirugía Valladolid 50:71–98
- Valencia S, Marín DE, Gómez D et al (2023) Spatio-temporal assessment of Gridded precipitation products across topographic and climatic gradients in Colombia. Atmos Res. https://doi.org/10.1016/j.atmosres .2023.106643
- Vicente-Serrano SM, Aguilar E, Martínez R et al (2017) The complex influence of ENSO on droughts in Ecuador. Clim Dyn 48:405–427. https://doi.org/10.1007/s00382-016-3082-y



165 Page 22 of 22 Climatic Change (2024) 177:165

World Meteorological Organization (2018) Guía de prácticas climatológicas

Yánez MP, Núñez M, Carrera F, Martínez C (2011) Posibles efectos del cambio climático global en zonas silvestres protegidas de la zona andina de Ecuador. La Granja Rev Ciencias La Vida 14:24–44

Zambrano-Bigiarini M (2017) Package 'hydroGOF". Goodness-of-fit Functions for Comparison of Simulated and Observed.'

Zambrano-Bigiarini M, Baez-Villanueva OM, Giraldo-Osorio J (2020) Merging of satellite datasets with ground observations using random forests

Zhang X, Yang F (2004) RClimdex (1.0): User Manual. 23

Zhiña D, Montenegro M, Montalván L et al (2019) Climate change influences of temporal and spatial Drought Variation in the Andean High Mountain Basin. Atmosphere (Basel) 10:558. https://doi.org/10 .3390/atmos10090558

Zhou B, Wen QH, Xu Y et al (2014) Projected changes in temperature and precipitation extremes in China by the CMIP5 multimodel ensembles. J Clim 27:6591–6611. https://doi.org/10.1175/JCLI-D-13-00761.1

Zuleta C, Arauz Calderón M (1998) Análisis estadístico De suma de precipitación y su correlación con formación de inundaciones en la costa ecuatoriana. Universidad Internacional SEK

Publisher's note Springer Nature remains neutral with regard to jurisdictional claims in published maps and institutional affiliations.

Springer Nature or its licensor (e.g. a society or other partner) holds exclusive rights to this article under a publishing agreement with the author(s) or other rightsholder(s); author self-archiving of the accepted manuscript version of this article is solely governed by the terms of such publishing agreement and applicable law.

Authors and Affiliations

Katy Valdivieso-García^{1,2} · Angel Vázquez-Patiño^{3,4,5} · Hugo Saritama · Juan Contreras · Alex Avilés^{1,2} · Fernando García^{1,2}

- Alex Avilés
 alex.aviles@ucuenca.edu.ec
- Carrera de Ingeniería Ambiental, Facultad de Ciencias Químicas, Eco Campus Balzay, Universidad de Cuenca, Av. Victor Albornoz y Calle de los Cerezos, 010207 Cuenca, Ecuador
- Grupo de Evaluación de Riesgos Ambientales en Sistemas de Producción y Servicios (RISKEN), Departamento de Química Aplicada y Sistemas de Producción, Eco Campus Balzay, Universidad de Cuenca, Av. Victor Albornoz y Calle de los Cerezos, 010207 Cuenca, Ecuador
- Department of Civil Engineering, University of Cuenca, Av 12 de Abril y Loja, Cuenca 010203, Ecuador
- Faculty of Engineering, University of Cuenca, Av 12 de Abril y Loja, Cuenca 010203, Ecuador
- Faculty of Architecture and Urbanism, University of Cuenca, Av 12 de Abril y Loja, Cuenca 010203, Ecuador
- Instituto de Estudios de Régimen Seccional del Ecuador (IERSE), Universidad del Azuay, Av. 24 de mayo 7-77 y Hernán Malo, 010204 Cuenca, Ecuador

